Modelling Simul. Mater. Sci. Eng. 1 (1993) 505–516. Printed in the UK

Kinetic modelling of diffusion-controlled, two-phase moving interface problems

Yunhong Zhou and Thomas H North
Department of Metallurgy and Materials Science, University of Toronto, Ontario, Canada

Received 24 July 1992, accepted for publication 29 October 1992

Abstract. A fast and accurate fully implicit finite difference model has been developed for the simulation of diffusion-controlled, two-phase, moving interface problems. The computed results are in good agreement with experimental values produced during transient liquid-phase bonding of nickel, and during solution treatment of thin, multiple layers of α and β brass. The present results are compared with the models proposed by other workers.

1. Introduction

Diffusion controlled moving boundary problems occur in a wide range of metallurgical situations [1]—in the solid-state (during growth and subsequent dissolution of a second phase in a solution treatment [2], during growth of intermediate layers in thermal barrier coatings [3]); and in a solid–liquid situation (during growth or/and shrinkage of the liquid phase in transient liquid phase (TLP) bonding [4,5] and in liquid phase sintering [6]). Although a number of investigators have modelled the growth of unstable phases [7–13], long calculation times are involved because of the explicit formulae used. This is an especially severe problem when an attempt is made to model a complex process such as transient liquid phase bonding (because the process time is extremely long compared with the calculation time step needed for stability of the numerical solution). As an example, computations of microsegregation during binary alloy casting took several days to perform using computer workstations [14].

In the present study, fully implicit, finite difference modelling is used to analyse diffusion-controlled, two-phase, moving interface problems, with the aim of decreasing the calculation time involved and increasing the accuracy of the final output. The validity of the computed results are compared directly with experimental results produced during transient-liquid phase bonding of single-crystal nickel, and solution treatment of thin, multilayer α and β brass diffusion couples [8].

1.1. Transient liquid phase bonding of nickel

TLP bonding is commonly used during the repair of aero-engine turbine blades. This joining process involves a series of steps, namely, base metal dissolution, liquid phase isothermal solidification, and solute homogenization [4,5]. The growth and shrinkage of the transitory liquid phase is determined by diffusion-controlled, solid–liquid interface migration. In the present study, detailed numerical modelling of TLP bonding is carried out by treating dissolution, isothermal solidification and homogenization as sequential steps. The calculation results are compared with the experimental results produced during TLP

0965-0393/93/040505+12$07.50

bonding of single-crystal nickel using Ni-19 at.% P filler metal. A detailed description of the experimental set-up during TLP bonding has been presented elsewhere [15] and consequently, only a brief description of the experimental procedure will be indicated here. 25 μm thick Ni-19 at.% P filler metal was clamped between the single-crystal nickel components and the joining operation was carried out at 1150 °C in a 10^{-5} torr vacuum. After a known holding time, the test specimens were quenched in an oil bath and the width of the liquid zone during isothermal solidification was evaluated using optical microscopy. The liquid width at the bonding temperature was calculated from the measured eutectic width using the procedure indicated by Nakao *et al* [16].

1.2. Solution treatment of α and β brass diffusion couples

When an α and β phase aggregate is solution-treated at a temperature where only α is stable, there will be a time-dependent transformation to the single-phase α structure. However, if there is a large flux in the β layer (due to large variations in solubility with temperature and/or to a large interdiffusion coefficient at the solution temperature) it is possible for the α/β interface to move initially so that the content of the β phase increases [8]. Finally, the β phase dissolves when the rapid loss of the supersaturation in the β phase occurs, and the final structure approaches the end point defined by the equilibrium phase diagram. This effect has been examined experimentally during solution treatment of thin, multiple layers of α and β brass diffusion couples by Heckel *et al* [8], and has been modelled by Tanzilli and Heckel [7]. In the present paper, the results produced using fully implicit, finite difference modelling are compared directly with Heckel and Tanzilli's experimental results and modelling output. The computation results are also compared with the values produced using Pabi's numerical model for simulating two-phase, diffusion-controlled dissolution [9].

2. Problem formulation

Figure 1 shows a schematic illustration of diffusion-controlled, two-phase, moving interface problems. Figure 1(a) shows a planar interface situation where constant-size zones of the solute-rich second phase are dispersed uniformly throughout the matrix. When this assembly is held at the solution temperature, the second phase grows and then dissolves [8]. Figure 1(b) illustrates the situation during TLP bonding, when the liquid phase grows and then disappears at the bonding temperature.

The basic assumptions during numerical modelling are: (1) the moving interface remains planar throughout the processing period; (2) the diffusion coefficient, molar volume and activity coefficient of the solute are independent of composition, while the molar volume in the different phases are also equal; (3) local equilibrium exists at the moving interface; and (4) there is negligible liquid flow due to convection and stirring (in the liquid phase) and there is no effect of latent heat on the temperature distribution and on movement of the solid–liquid interface.

Figure 2 shows the solute concentration, $c(x, t)$, and the moving interface location, $X(t)$. The second-phase region is at $0 \leqslant x \leqslant X(t)$ and the matrix region is at $X(t) \leqslant x \leqslant L/2$. The width of the second phase is $w(t) = 2X(t)$. The governing equations which determine solute diffusion field are:

$$\frac{\partial c_p(x,t)}{\partial t} = D_p \frac{\partial^2 c_p(x,t)}{\partial x^2} \qquad 0 \leqslant x \leqslant X(t) \tag{1}$$

$$\frac{\partial c_m(x,t)}{\partial t} = D_m \frac{\partial^2 c_m(x,t)}{\partial x^2} \qquad X(t) \leqslant x \leqslant \frac{L}{2}. \tag{2}$$

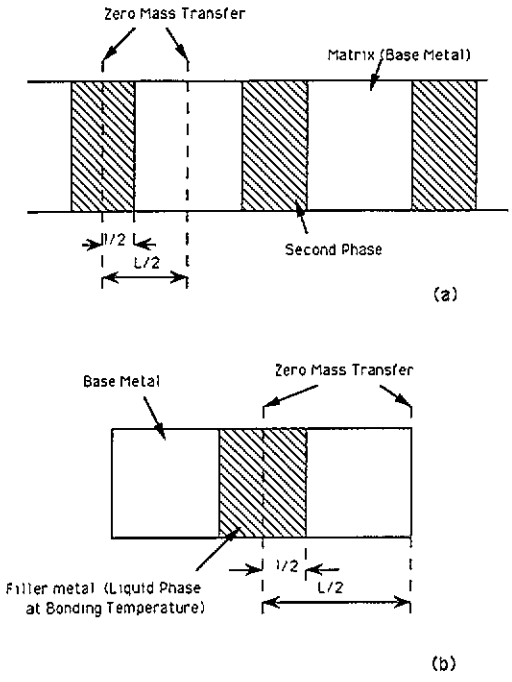

Figure 1. (*a*) Schematic illustrating modelling of the α and β brass solution treatment (after [9]); (*b*) schematic illustrating TLP bonding of nickel.

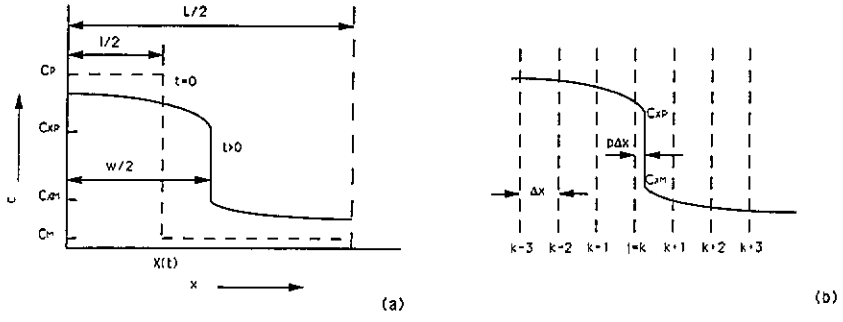

Figure 2. (*a*) Concentration profile produced by interface movement. The dashed lines show the situation at $t = 0$ and the solid lines show the situation at $t > 0$; (*b*) the numerical method employed to analyse movement of the interface.

Where the subscripts p and m indicate the second and matrix phases respectively, and D is the diffusion coefficient. These are subject to the following boundary conditions,

$$\left.\frac{\partial c_{\mathrm{p}}(x,t)}{\partial x}\right|_{x=0} = 0 \tag{3}$$

$$\left.\frac{\partial c_{\mathrm{m}}(x,t)}{\partial x}\right|_{x=L/2} = 0. \tag{4}$$

The initial conditions are (from figure 2)

$$c_p(x,0) = C_P \qquad 0 \leqslant x \leqslant l/1 \tag{5}$$

$$c_m(x,0) = C_M \qquad l/2 \leqslant x \leqslant L/2 \tag{6}$$

where C_M is the initial solute concentration in the base metal. At the moving interface

$$c_p(X(t),t) = C_{XP} \tag{7}$$

$$c_m(X(t),t) = C_{XM} \tag{8}$$

where C_{xm} is the solute concentration of the matrix at the moving interface, and because of the conservation of mass at the moving interface, the interface movement is determined by the relation:

$$(C_{XP} - C_{XM})\frac{dX(t)}{dt} = -D_p \frac{\partial c_p(x,t)}{\partial x}\bigg|_{x=X(t)} + D_m \frac{\partial c_m(x,t)}{\partial x}\bigg|_{x=X(t)} \tag{9}$$

3. Numerical analysis

The approach taken involves using the finite difference approximation to obtain discrete forms of differential equations (1), (2) and (9), with finite boundary and initial conditions. As a first step, an implicit finite difference method was employed when approximating (1) and (2) in order to decrease the calculation time (this overcomes the stability restriction on the maximum time step). Equation (9) was solved using the explicit method in [7–14] and the accuracy of the solution decreased when large time steps were employed. In the present paper, (9) was solved using an implicit method. As a result, a fully implicit scheme has been developed which handles diffusion controlled, moving interface problems.

3.1. Approximating the diffusion equations

The space domain is divided into H equally-spaced intervals of length Δx, namely, $x_j = (j-1)\Delta x$, $j = 1, 2, 3, \ldots, H+1$, where j represents some mesh point, and $\Delta x = L/2H$. The interface lies between the nodes $j = k$ and $k+1$, and $p = \{X(t) - (k-1)\Delta x\}/\Delta x$, where $0 \leqslant p \leqslant 1$ and $k = 1, 2, 3, \ldots$ (see figure 2(*b*)). The time step varies with the interface velocity at a constant interface displacement $\Delta t = E\Delta x/(dX/dt)$, where E is a constant. Since the interface moves very quickly in the initial period and then slows down, this treatment ensures that the time step will be small enough (in the initial stage) that the calculation accuracy will be acceptable. The finite difference expression for (1) and (2) is:

$$\frac{c_j^{t+\Delta t} - c_j^t}{\Delta t} = D\frac{\theta(\delta^2 c)_j^{t+\Delta t} + (1-\theta)(\delta^2 c)_j^t}{(\Delta x)^2} \tag{10}$$

where $(\delta^2 c)_j = c_{j+1} - 2c_j + c_{j-1}$, for the nodes $j = 2, 3, \ldots, H$; except for the nodes near the moving interface. Using the zero-flux boundary conditions in (3) and (4), at the boundary nodes $j = 1$ and $H+1$, one can obtain,

$$(\delta^2 c)_1 = 2(c_2 - c_1) \tag{11}$$

$$(\delta^2 c)_{H+1} = 2(c_H - c_{H+1}). \tag{12}$$

Near the moving interface [17]:

$$(\delta^2 c)_k = 2\left(\frac{c_{k-1}}{1+p} - \frac{c_k}{p} + \frac{c_{XP}}{p(1+p)}\right) \tag{13}$$

$$(\delta^2 c)_{k+1} = 2\left(\frac{c_{XM}}{(1-p)(2-p)} - \frac{c_{k+1}}{(1-p)} + \frac{c_{k+2}}{(2-p)}\right). \tag{14}$$

Equations (10)–(14) comprise two sets of equations, one (from $j = 1$ to k) for the second-phase region, and the other (from $j = k+1$ to H) for the base-metal region. However, (13) and (14) have singularities at $p = 0$ in (13) and $p = 1$ in (14). This singular behaviour is handled using the following approach: when $p < \frac{1}{2}$, the equation set extends from $j = 1$ to $k - 1$ for the second-phase region, and c_k can be calculated using the finite-difference expression (assuming that the concentration on both sides of the moving interface are described by quadratic relations)

$$(\delta^2 c)_{k-1} = 2\left(\frac{c_{k-2}}{2+p} - \frac{c_{k-1}}{1+p} + \frac{C_{XP}}{(1+p)(2+p)}\right) \tag{15}$$

$$c_k = -\frac{pc_{k-2}}{2+p} + \frac{2pc_{k-1}}{1+p} + \frac{2C_{XP}}{(1+p)(2+p)}. \tag{16}$$

When $p > \frac{1}{2}$, the equation set extends from $j = k+2$ to H for the base-metal region,

$$(\delta^2 c)_{k+2} = 2\left(\frac{C_{XM}}{(2-p)(3-p)} - \frac{c_{k+2}}{(2-p)} + \frac{c_{k+3}}{(3-p)}\right) \tag{17}$$

and c_{k+1} is given as:

$$c_{k+1} = \frac{2C_{XM}}{(2-p)(3-p)} + \frac{2(1-p)c_{k+2}}{(2-p)} - \frac{(1-p)c_{k+3}}{(3-p)}. \tag{18}$$

θ in (10) is a weighted constant, and the solution is unconditionally stable and convergent when $\frac{1}{2} \leqslant \theta \leqslant 1$. However, for $1 \leqslant \theta < \frac{1}{2}$, we must employ the relation:

$$\frac{D\Delta t}{(\Delta x)^2} \leqslant \frac{1}{2(1-2\theta)}. \tag{19}$$

This stability restriction on the maximum time step requires an enormous number of calculation cycles during problem solution. In this work, the θ value is taken as $\frac{1}{2} - (\Delta x)^2/12D\Delta t$, where θ is taken as 0 for all values of $\theta < 0$ at the initial stage, when the velocity of the moving interface is very fast and the time step must be small). This special scheme has a truncation error of $O(\Delta t^2 + \Delta x^4)$ [18]. This is smaller than that at $\theta = 0$ (for an explicit scheme), $\theta = 1$ (for an implicit scheme) and even $\theta = 0.5$ (using the Crank–Nicolson scheme [17]). The solution is also stable. Another advantage of the implicit scheme is that there are no stability restrictions regarding time-step selection. This means that the calculation time can be decreased without affecting the solution stability.

3.2. Approximating the moving interface

Rearranging (9) gives

$$\frac{\mathrm{d}X(t)}{\mathrm{d}t} = \frac{1}{C_{XP} - C_{XM}}\left(-D_p \frac{\partial c_p(x,t)}{\partial x}\bigg|_{x=X(t)} + D_m \frac{\partial c_m(x,t)}{\partial x}\bigg|_{x=X(t)}\right)$$
$$= f[X(t), t]. \tag{20}$$

The modified Euler method (implicit scheme) is applied to solve (20), namely

$$X^{(0)}(t + \Delta t) = X(t) + \Delta t f[X(t), t] \tag{21}$$

$$X^{(n+1)}(t + \Delta t) = X(t) + (\Delta t/2)\{f[X(t), t] + f[X^{(n)}(t + \Delta t), t + \Delta t]\} \tag{22}$$

where $n = 0, 1, 2, \ldots$, and the iteration at each time step is performed until:

$$\left|\frac{X^{(n+1)}(t + \Delta t) - X^{(n)}(t + \Delta t)}{X^{(n)}(t + \Delta t)}\right| < 10^{-6}. \tag{23}$$

This implicit scheme for (20) improves the calculation accuracy, the error is $O(\Delta t^3)$ [19] and much larger time steps are therefore allowed.

The treatment applied to (13) and (14) can be used to approximate the derivatives in (20). When $p > \frac{1}{2}$

$$\frac{\partial c_p}{\partial x}\bigg|_{x=X} = \frac{1}{\Delta x}\left(\frac{pc_{k-1}}{1+p} - \frac{(1+p)c_k}{p} + \frac{(1+2p)C_{XP}}{p(1+p)}\right) \tag{24}$$

$$\frac{\partial c_m}{\partial x}\bigg|_{x=X} = \frac{1}{\Delta x}\left(\frac{(2p-5)C_{XP}}{(2-p)(3-p)} + \frac{(3-p)c_{k+2}}{(2-p)} - \frac{(2-p)c_{k+3}}{(3-p)}\right) \tag{25}$$

and when $p < \frac{1}{2}$

$$\frac{\partial c_p}{\partial x}\bigg|_{x=X} = \frac{1}{\Delta x}\left(\frac{(1+p)c_{k-2}}{2+p} - \frac{(2+p)c_{k-1}}{1+p} + \frac{(3+2p)C_{XP}}{(1+p)(2+p)}\right) \tag{26}$$

$$\frac{\partial c_m}{\partial x}\bigg|_{x=X} = \frac{1}{\Delta x}\left(\frac{(2p-3)C_{XM}}{(1-p)(2-p)} + \frac{(2-p)c_{k+1}}{(1-p)} - \frac{(1-p)c_{k+2}}{(2-p)}\right) \tag{27}$$

3.3. Initiating the solution

Since the numerical solution cannot be initiated directly using the initial conditions (in (5) and (6)) an approximate analytical solution for a very small time step is used as the starting point for the finite difference scheme, i.e.

$$X(\Delta t) = \tfrac{1}{2}l + 2\beta\sqrt{\Delta t}. \tag{28}$$

In (21), β is calculated using (A12) in the appendix and is a constant which depends on the material properties (on the solute diffusivity and solubility values).

The numerical computation proceeds as follows.

(i) The initial movement of the interface is calculated using (28).

(ii) The new solute concentration distribution at each nodal point, after the initial interface movement, is calculated using the discrete forms of (1) and (2).

(iii) The new moving interface position is calculated starting from the previous position, using the discrete form of (9).

(iv) The redistribution of solute from the previous concentration at each nodal point is calculated using the discrete forms of (1) and (2).

(v) Steps (iii) and (iv) are repeated until the process is completed.

4. Results and discussion

The normalized thickness of the second phase (w/l), where ω is the width of the second phase and l is its width initially, is plotted as a function of dimensionless time (Dt/l^2). The optimum calculation conditions that produced satisfactory results were evaluated by a trial and error procedure. Different mesh size and E values were selected and tested until no major changes in results were produced when finer Δx and E values were substituted. The effectiveness of the computations was evaluated by comparing the calculated values with the experimental results produced during solution treatment of α and β brass, and during TLP bonding of single-crystal nickel. The parameters employed in the calculations are listed in table 1.

Table 1. Input parameters for numerical modelling.

Curve no.	C_M (at.%)	C_{XM} (at.%)	C_{XP} (at.%)	C_P (at.%)	D_m ($\mu m^2\ s^{-1}$)	D_p ($\mu m^2\ s^{-1}$)	l (μm)	L (μm)	Δx (μm)	E
2[a]	0.0	0.166	10.223	19.0	18.0	500.0	25.0	6025.0	1.0	0.01
3[b]	29.1	32.5	36.9	39.4	5.0	100.0	381.0	1134.0	10.0	0.1
4-a[c]	0.0	0.4	0.9	1.0	0.0603	0.0603	0.44	1.321	0.01	0.1
4-b[d]	0.0	0.1	0.6	1.0	0.0603	0.0603	0.44	18.033	0.01	0.1
4-c[e]	0.0	0.1	0.9	1.0	0.0603	0.0603	0.44	18.033	0.01	0.1

[a]: Alloy system, Ni-P [16,20].
[b]: Alloy system, α-brass/β-brass [8].
[c]: Alloy system, hypothetical [9].
[d]: Alloy system, hypothetical [9].
[e]: Alloy system, hypothetical [9].

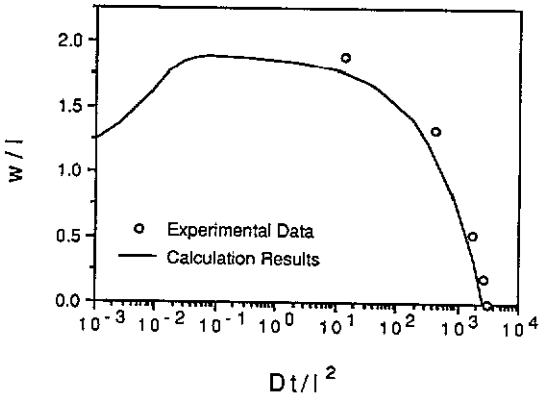

Figure 3. Comparison of the calculated and experimental results during TLP bonding of single-crystal nickel.

4.1. Comparison of calculated results with experimental values produced during TLP bonding of nickel

Figure 3 compares the output of the computer model with the experimental results produced during TLP bonding of single-crystal nickel base metal. The experimental values are in good

agreement with the computed results, bearing in mind the difficulties in obtaining an accurate diffusion coefficient value for phosphorus in the liquid phase, and the errors caused by the assumption that the diffusion coefficients are independent of composition. It is important to point out that the excellent correspondence between calculated and experimental results occurs only when a single-crystal nickel base metal is employed during TLP bonding. During modelling, it was assumed that there was no effect of grain boundary regions on movement of the solid–liquid interface. When fine-grained nickel base metal is employed during TLP bonding, there is a marked effect of grain boundaries on the rate of completion of the isothermal solidification stage (the rate of isothermal solidification increases when the grain size of the base metal decreases [15, 21]). Faster isothermal solidification occurs since liquid penetration at grain boundaries in the nickel base metal increases the area at the solid–liquid interface and promotes solute diffusion into the base metal. This liquid penetration feature has been modelled recently by Ikeuchi *et al* [22] and depends on the grain boundary energy, and on the energy balance between the grain boundary and the solid–liquid interface.

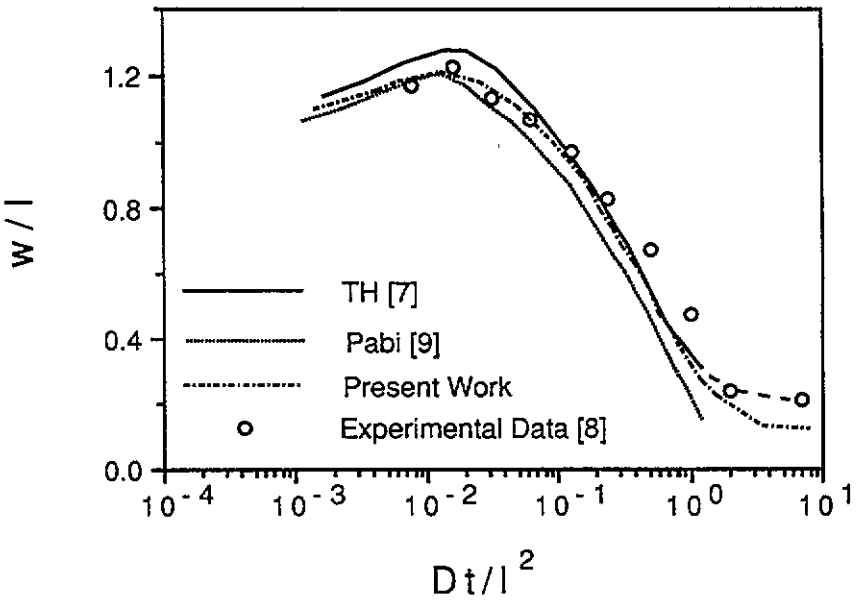

Figure 4. Comparison of the calculated and experimental results during solution treatment of thin, multilayer α and β brass diffusion couples (using the experimental results presented in [8]).

4.2. Comparison of calculated and experimental results during solution treatment of α and β brass diffusion couples

Figure 4 compares the output of our model with the experimental results [8] and model calculations produced by Tanzilli and Heckel [7] and Pabi [9]. Our computed results show a better fit with the experimental results than the TH model (Tanzilli and Heckel) and Pabi's model, although some deviation is apparent late in the solution process. The difference between the calculated and experimental results may be attributed to errors in ascribing solubility and diffusion coefficient values, and to experiment errors. In addition, the TH

model indicates a larger amount of transient growth and Pabi's model [9] indicates faster solution kinetics late in the solution process.

The output of the different models can also be compared by applying the hypothetical input values suggested by Pabi [9], namely:

(i) when the interface flux to the matrix exceeds that from the dissolving phase, there is no second-phase growth (this is curve (a) in figure 5);

(ii) when (D_m/D_p) and $(C_p - C_{XP})/(C_{XM} - C_M)$ are both unity, the interface movement is zero for a short time period and then the second phase dissolves monotonically (this is curve (c) in figure 5);

(iii) when the flux in the second phase exceeds that in the matrix, the second phase grows and then dissolves (this is curve (b) in figure 5).

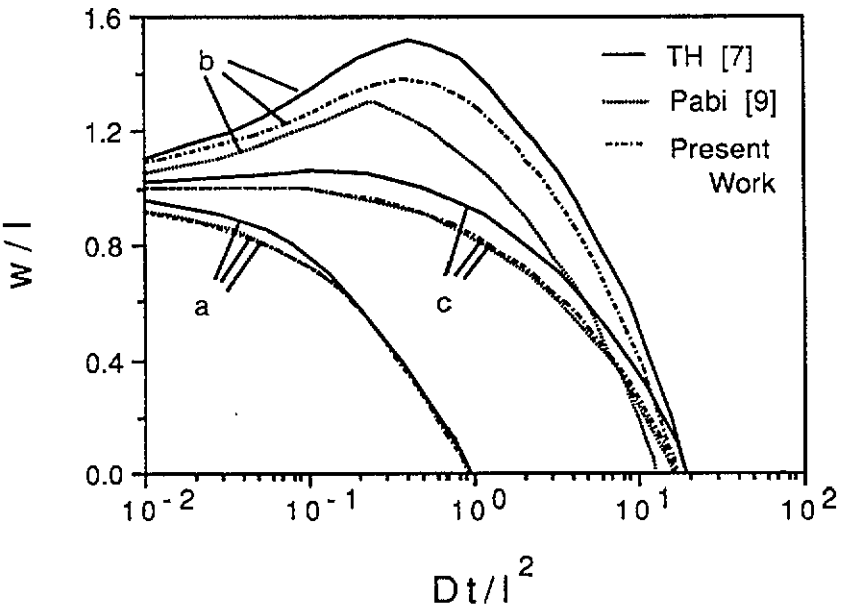

Figure 5. Comparison of the output of the different computational models (TH—Tanzilli and Heckel's model [7] and Pabi's model [9]).

The output of our model closely corresponds with that produced using Pabi's model (in curves (a) and (c)). However, the TH model indicates an erroneous transient growth in curve (c) because of errors in the slope calculation (due to the unequal grid size in the different phases) [9]. When transient second-phase growth occurs (curve (b)), our model produces a better prediction than the other models; this is also apparent in figure 4.

4.3. Calculation time

The cpu times involved in these computations were compared at $\theta = 0$ (in the explicit scheme) and $\theta = \frac{1}{2} - (\Delta x)^2/12D\Delta t$ (in the implicit scheme) using a Silicon Graphics IRIS 4.0.1 mini-computer. The cpu times were 400 and 7.9 s respectively (for curve a in figure 5). In the explicit case, the time step was limited to 8.0×10^{-4} s and about 7.0×10^4 cycles were required to complete the calculations. Using the implicit method, the time steps ranged

from 1.85×10^{-5} to 0.285 s and about 400 cycles were needed to complete the calculations. Although this difference in cpu time does not appear considerable, it is extremely important when TLP bonding of nickel is modelled. When TLP bonding is modelled, the fully implicit scheme required three minutes of cpu time, the calculation time steps range from 8.6×10^{-4} to 70 s, and the number of calculation cycles is around 3500. However, when the explicit scheme is used, the time step must be less than 10^{-3} s, the total process time is around 9.0×10^{5} s and 10^{8} calculation cycles are required during modelling.

5. Summary

A fast and accurate, fully implicit finite difference model has been developed which simulates diffusion-controlled, two-phase, moving-interface problems. The computed results are in good agreement with the experimental results produced during TLP bonding of single-crystal nickel, and during the solution treatment of thin, multilayer α and β brass diffusion couples. The model developed in this study produces results which compare well with the output of the numerical models proposed by Tanzilli and Heckel [7] and Pabi [9].

Acknowledgments

The authors wish to acknowledge the Ontario Centre for Materials Research (OCMR) and the Welding Research Council (New York) for financial support during the prosecution of this research program. Also, the authors wish to acknowledge the considerable contribution by W Fearis in regard to the TLP bonding experiments. In addition, the authors would like to acknowledge the invaluable contribution made by Dr Kenji Ikeuchi (Welding Research Institute, Osaka University) in patiently discussing this modelling research effort.

Appendix

The analytical solution for a diffusion problem which involves two phases separated by a moving planar interface has been given by Danckwerts [23]. For semi-infinite media, where two phases meet at the moving interface $X(t)$

$$\frac{\partial c_p(x,t)}{\partial t} = D_p \frac{\partial^2 c_p(x,t)}{\partial x^2} \qquad -\infty \leqslant x \leqslant X(t) \tag{A1}$$

$$\frac{\partial c_m(x,t)}{\partial t} = D_m \frac{\partial^2 c_m(x,t)}{\partial x^2} \qquad X(t) \leqslant x \leqslant \infty. \tag{A2}$$

When the error function solution is applied to each phase,

$$c_p(x,t) = A_1 + A_2 \operatorname{erf}\left(x/2\sqrt{D_p t}\right) \tag{A3}$$

$$c_m(x,t) = A_3 + A_4 \operatorname{erf}\left(x/2\sqrt{D_m t}\right). \tag{A4}$$

A_1, A_2, A_3 and A_4 are constants. Using the appropriate boundary conditions, we obtain

$$c_p(\infty,t) = A_1 + A_2 = c_\infty \tag{A5}$$

$$c_m(-\infty,t) = A_3 + A_4 = c_{-\infty}. \tag{A6}$$

At the moving interfaces, we have

$$c_m(X,t) = A_1 + A_2\,\mathrm{erf}\left(X/2\sqrt{D_m t}\right) = C_{XM} \tag{A7}$$

$$c_p(X,t) = A_3 + A_4\,\mathrm{erf}\left(X/2\sqrt{D_p t}\right) = C_{XP}. \tag{A8}$$

Since (A7) and (A8) have to be satisfied for all values of t, X must be proportional to $\sqrt{t}$, i.e.

$$X = 2\beta\sqrt{t}. \tag{A9}$$

Substituting (A1)–(A9) in the equation governing interface movement,

$$\left(C_{XP} - C_{XM}\right)\frac{\mathrm{d}X(t)}{\mathrm{d}t} = -D_p\frac{\partial c_p(x,t)}{\partial x}\bigg|_{x=X(t)} - D_m\frac{\partial c_m(x,t)}{\partial x}\bigg|_{x=X(t)} \tag{A10}$$

and we can derive

$$\left(C_{XP} - C_{XM}\right)\beta\sqrt{\pi} - \frac{\sqrt{D_p}(c_{-\infty} - C_{XP})}{1 + \mathrm{erf}(\beta/\sqrt{D_p})}\exp\left(-\frac{\beta^2}{D_p}\right) + \frac{\sqrt{D_m}(C_{XM} - c_\infty)}{1 - \mathrm{erf}(\beta/\sqrt{D_m})} \times \exp\left(-\frac{\beta^2}{D_m}\right) = 0. \tag{A11}$$

At the very beginning of the dissolution process, the liquid and solid phases can be approximated as infinite mediums, i.e. $c_{-\infty} = C_P$ and $c_\infty = C_M$ and (A11) becomes:

$$\left(C_{XP} - C_{CM}\right)\beta\sqrt{\pi} - \frac{\sqrt{D_p}(C_P - C_{XP})}{1 + \mathrm{erf}(\beta/\sqrt{D_p})}\exp\left(-\frac{\beta^2}{D_p}\right) + \frac{\sqrt{D_m}(C_{XM} - C_M)}{1 - \mathrm{erf}(\beta/\sqrt{D_m})} \times \exp\left(-\frac{\beta^2}{D_m}\right) = 0. \tag{A12}$$

After calculating β from (A11), (A9) traces the movement of the interface.

Nomenclature

A_1, A_2, A_3, A_4	constants
c and C	solute concentration (at.%)
C_P	initial solute concentration in second phase (at.%)
C_M	initial solute concentration in base metal (at.%)
C_{XP}	solute concentration of second phase at the moving interface (at.%)
C_{XM}	solute concentration of matrix at the moving interface (at.%)
D	diffusion coefficient ($\mu m^2\ s^{-1}$)
I	initial width of second phase (μm)
p	$\{X(t) - (k-1)\Delta x\}/\Delta x$
t	time variable (s)
x	space variable (μm)
X	moving interface position (μm)
w	width of second phase (μm)
Δ	increment of variables
β	constant

Subscripts

p	indicates second phase
m	indicates matrix phase
j	current mesh point

References

[1] Sekerka R F, Jeanfils C L and Heckel R W 1975 The moving boundary problem *Lectures on the Theory of Phase Transformations* ed H I Aaronson (New York: AIME) pp 117–69
[2] Tanzilli R A and Heckel R W 1971 *Metall. Trans.* **2** 1779–84
[3] Bhanumurthy K, Kale G B, Khera S K and Asundi M K 1990 *Metall. Trans.* A **21** 2897–903
[4] Duall D S, Owczarski W A and Paulonis D F 1974 *Welding J.* **53** 203–14
[5] Tuah-Poku I, Dollars M and Massalsi T B 1988 *Metall. Trans.* A **19** 675–86
[6] Kaysser W A, Huppmann W J and Petzow G 1980 *Powder Metall.* **23** 86–91
[7] Tanzilli R A and Heckel R W 1968 *Trans. AIME* **242** 2313–21
[8] Heckel R W, Hickl A J, Zaehring R J and Tanzilli R A 1972 *Metall. Trans.* **3** 2565–9
[9] Pabi S K 1979 *Phys. Status Solidi* **51** 281–9
[10] Lanam R D and Heckel R W 1971 *Metall. Trans.* **2** 2255–66
[11] Karlsson B and Larsson L-E 1975 *Mater. Sci. Eng.* **20** 161–70
[12] Nakagawa H, Lee C H and North T H 1991 *Metall. Trans.* A **22** 543–55
[13] North T H, Ikeuchi K, Zhou Y and Kokawa H 1991 Dissolution and isothermal solidification in transient liquid phase brazing *TMS Symp., The Metal Science of Joining (Cincinnati, 1991)* pp 83–91
[14] Battle T P and Pehlke R D 1990 *Metall. Trans.* B **21** 357–74
[15] Saida K, Zhou Y and North T H 1992 The influence of base metal grain size on isothermal solidification during TLP-brazing of nickel, unpublished
[16] Nakao Y, Nishimoto K, Shinozaki K and Kang C Y 1990 Advanced joining technologies *Joining of Advanced Materials* ed T H North pp 129–44
[17] Crank J 1984 *Free and Moving Boundary Problems* (Oxford: Oxford University Press)
[18] Richtmyer R D 1957 *Difference Methods for Initial-value Problems* (New York: Interscience)
[19] Gerald C F and Wheatly P O 1989 *Applied Numerical Analysis* 4th edn (New York: Addison-Wesley)
[20] Nash P (ed) 1991 *Phase Diagrams of Binary Nickel Alloys* (Ohio: ASM) pp 235
[21] Kokawa H, Lee C H and North T H 1991 *Metall. Trans.* A **22** 1627–31
[22] Ikeuchi K, Zhou Y, Kokawa H and North T H 1992 *Metall. Trans.* A **23** pp 2905–15
[23] Danckwerts P V 1950 *Trans. Faraday Soc.* **46** 701–12